

Double $1s$ shell ionization of Si induced in collisions with 1–3-MeV protons

M. Kavčič*

J. Stefan Institute, P.O. Box 3000, SI-1001, Ljubljana, Slovenia and Physics Department, University of Fribourg, CH-1700 Fribourg, Switzerland

K. Tökési

Institute of Nuclear Research of the Hungarian Academy of Science (ATOMKI), H-4001 Debrecen,

P.O. Box 51, Hungary

(Received 13 September 2005; published 9 December 2005)

The double $1s$ ionization of Si induced in collisions with protons was studied by measuring the K x-ray emission of a solid Si target ionized by the impact of 1–3-MeV protons. In order to resolve the hypersatellite contributions corresponding to the radiative decay of the double $1s$ vacancy state, a high-resolution crystal spectrometer was employed yielding sub-eV energy resolution. From the intensity of the measured hypersatellite lines double $1s$ ionization cross sections for the studied collisions were determined. Experimental values were compared with the theoretical ones obtained within the independent electron framework employing single electron ionization probabilities calculated with the semiclassical approach. This comparison suggests a sequential two step model for the double $1s$ ionization which was additionally confirmed by four body classical trajectory Monte Carlo calculations.

DOI: [10.1103/PhysRevA.72.062704](https://doi.org/10.1103/PhysRevA.72.062704)

PACS number(s): 34.50.Fa, 32.30.Rj, 32.70.Fw, 32.80.Hd

I. INTRODUCTION

The radiative de-excitation of the double $1s$ vacancy states of atoms induced in collisions with charged particles (electrons, ions) or photons corresponds to the hypersatellite spectral lines in the K x-ray emission spectra. Because of the reduced nuclear charge screening due to additional vacancy in the $1s$ shell, the hypersatellites are shifted towards higher energies as compared to the parent diagram lines corresponding to the radiative decay of single $1s$ vacancy state. Measured intensity of the hypersatellite lines gives us the possibility to determine the double $1s$ ionization cross sections for the studied collisions.

Among different excitation possibilities leading to double $1s$ ionization, the highest cross sections are observed in collisions with heavy ions in which relatively strong K hypersatellites have been measured [1]. But the problem encountered with heavy ions is the high probability for additional ionization of outer shells resulting in complex x-ray spectra from which it is very difficult to resolve properly the hypersatellites and extract out the double $1s$ ionization cross sections. In addition for such rather symmetric collisions we have two ionization mechanisms both contributing to the measured hypersatellite intensity, the direct Coulomb ionization and the capture of inner-shell electrons into the empty shells of the projectile (electron transfer). A detailed investigation of the relative importance of the two main ionization mechanisms has been done for example by Hall and co-workers [2,3] for Ti bombarded by heavy ions.

On the other hand, in experiments with protons, where additional outer-shell ionization is less probable, hypersatellites are well isolated resulting in relatively accurate deter-

mination of the double ionization cross sections as it has been done for some low Z elements [4]. A similar method has been used in the case of helium ions on mid- Z atoms [5] where additional outer-shell ionization also played a negligible role. Furthermore, as we have only direct ionization contribution, the assumption that multiple ionization induced in ion-atom collisions can be treated as a product of uncorrelated single ionization processes can be further probed by comparison with theoretical calculations within independent electron framework. Both previously mentioned studies [4,5] found that the theory overestimates the experimental values and at least part of these discrepancies were assigned to the proper description of the collision. Instead of the simultaneous ejection of two $1s$ electrons a sequential two-step process was suggested in which the binding energy of the second $1s$ electron should be increased due to the removal of the first one. As the difference between the two pictures increases by decreasing the Z of the measured element accurate double ionization cross-section data for even lighter elements is very appropriate to further test this assumption.

Usually in experiments where hypersatellites were measured the double to single $1s$ ionization cross-section ratio was determined from the intensity ratio of the $K\alpha$ hypersatellite and diagram line. But in case of Si the energy shift of the $K\alpha$ hypersatellite line relative to the diagram one is approximately 134 eV so the hypersatellite line is shifted above the K absorption edge increasing significantly the self-absorption in the solid target. As a result hypersatellite lines are heavily suppressed compared to the diagram ones. Additional difficulty is the partial overlap of the hypersatellite with the $K\beta L$ satellite lines so the high-energy experimental resolution is mandatory to resolve the hypersatellite contribution. As a result of this difficult experimental conditions quantitative experimental data about double $1s$ shell ionization of Si induced in ion-atom collisions are extremely scarce.

*Corresponding author. Email addresses: matjaz.kavcic@unifr.ch, matjaz.kavcic@ijs.si

In the present study our recent work about double $1s$ ionization of Si and Mg induced in collisions with heavy ions [6] was extended to asymmetric collisions using lighter projectiles, namely protons. We have used a high-resolution Johansson-type crystal spectrometer to measure the $K\alpha^h$ hypersatellite line of Si induced in collisions with 1–3-MeV protons. To avoid hypersatellite intensity normalization to the intensity of the $K\alpha$ diagram line the $K\beta L^1$ satellite line, which lies in close vicinity of the $K\alpha$ hypersatellite one, was used. The double to single $1s$ ionization cross section was derived from the measured intensity ratio of the $K\alpha^h$ hypersatellite and $K\beta L^1$ satellite lines, using the previously measured $K\alpha L^1/K\alpha L^0$ intensity ratio also obtained in collisions with 1–3-MeV protons [7]. Experimental values have been compared with the theoretical predictions obtained within the independent electron model using single $1s$ ionization probabilities calculated with the semiclassical approximation.

II. EXPERIMENT

The experiment was performed at the Microanalytical Centre (MIC) of the J. Stefan Institute, Ljubljana. Protons were accelerated by a 2-MV tandem accelerator. A thick Si target was bombarded with 1-, 2-, and 3-MeV protons. Beam current on the target depended slightly on the proton energy and it was $0.8 \mu\text{A}$ for the 1-MeV, $1.3 \mu\text{A}$ for the 2-MeV, and $0.8 \mu\text{A}$ again for the 3-MeV proton beam, respectively. Typical acquisition times for a single hypersatellite spectrum were 10–14 h.

The x rays emitted from the target after bombardment with protons were measured with the high-resolution crystal spectrometer in Johansson geometry. The spectrometer consists of a target holder, a target shielding which prevents the emitted x rays to reach the detector directly, a bent diffraction crystal, and a charge-coupled device (CCD) camera for the position sensitive detection of the diffracted x rays. The whole spectrometer is enclosed in a $1.6 \times 1.3 \times 0.4\text{-m}^3$ stainless-steel chamber evacuated by a turbomolecular pump down to 10^{-6} mbar.

The proton incidence and x-ray emission angle relative to the target surface was 45° . Emitted photons were reflected in the first order of reflection by the $(1\bar{1}0)$ reflecting planes of the SiO_2 crystal ($2d=8.5096 \text{ \AA}$). The Rowland circle radius of the crystal was 500 mm and the crystal size was 70 mm (width) \times 30 mm (height). After the diffraction on the crystal the photons were detected by a CCD camera, which was thermoelectrically cooled down to -40°C . The camera consisted of 770×1152 pixels, each having a size of $22.5 \times 22.5 \mu\text{m}^2$. The diffracted x rays generated a two-dimensional diffraction pattern on the CCD camera. Since the horizontal axis corresponds to the energy axis of the spectrum, the measured pattern was projected on the horizontal axis to get the final spectrum. The vertical extension served therefore merely to increase the collection area. For reducing the low-energy background a 6- μm mylar foil was inserted in front of the CCD detector.

In order to use the whole length of the CCD camera and measure a finite energy interval at the fixed detector position, the target was placed well inside the Rowland circle at a

distance of 37 cm in front of the diffraction crystal. To get the optimal energy resolution, the detector needs to be placed on the Rowland circle where the focusing condition is fulfilled. In our case the distance between the crystal and the detector was 821 mm, yielding finally an energy acceptance of 31 eV at a fixed detector position which was enough to cover the whole energy interval of interest without moving the detector. For the 2-MeV measurements, however, the spectrum was observed over three CCD lengths in order to get also the $K\beta_{1,3}$ diagram line in the measured energy interval. The $K\beta_{1,3}$ line serves us then as a reference line for the energy calibration. The energy of the reference line was set to 1835.96 eV [8]. The final experimental energy resolution, determined from the measurement of the $K\alpha_{1,2}$ line, was 0.35 eV. This resolution was good enough to resolve the K^2L^0 hypersatellite line from the $K\beta L^1$ satellite line.

III. DATA ANALYSIS

The measured spectrum induced with 2-MeV protons is presented in Fig. 1. Besides the $K\beta_{1,3}$ diagram line a weak structure is observed in the energy region 1850–1885 eV, presented in the inset of Fig. 1. For the identification of the three main components of this structure we can refer to our recently measured hypersatellite spectra induced in collisions with heavy ions [6] which were successfully decomposed using the theoretical line shapes calculated with the GRASP92 code. These calculations revealed that the first doublet of the structure correspond to the $K\beta L^1$ satellite line ($1s2p \rightarrow 3p2p$ transition) whether the third line is in fact a $K\alpha^h$ hypersatellite line ($1s^2 \rightarrow 2p1s$). This is confirmed also by comparing the spectra induced with three different proton energies (Fig. 2). While the relative intensity of both lines within the doublet corresponding to the $K\beta L^1$ satellite line shows no dependence on the proton energy, as expected since they correspond to the same ($1s2p \rightarrow 3p2p$) transition, the intensity of the hypersatellite line relative to the $K\beta L^1$ satellite one changes with the energy of the proton beam as the ratio of the double to single $1s$ ionization cross section is changing.

As it was already explained in the introduction the $K\alpha^h/K\beta L^1$ intensity ratio was used to obtain the double to single $1s$ ionization cross-section ratio. In order to extract the relative yield of the $K\beta L^1$ and $K\alpha^h$ lines for the three measured collisions we have fitted the spectra with three Voigt profiles which is a convolution of a Gaussian and Lorentzian corresponding to the instrumental response of the spectrometer and the natural line shape, respectively. The Gaussian width was fixed to 0.35 eV corresponding to our experimental resolution while other parameters were let free in the fit. With this model we were able to successfully fit the measured spectra and extract the intensity ratio of the measured components (Fig. 2). A good agreement was found between the energy of the Si hypersatellite line obtained from the fit (1873.6 ± 0.1 eV) and the result of the recent calculation by Martins *et al.* [9] (1874 eV) confirming the validity of the fitting model. It is also interesting to note the Lorentzian width of the measured hypersatellite line which was found to be $2.3 \text{ eV} \pm 0.2 \text{ eV}$. As expected due to the double vacancy

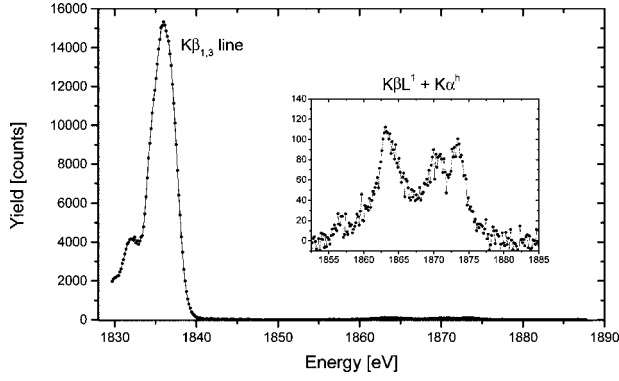


FIG. 1. High-resolution $K\beta$ x-ray spectrum of Si induced in collisions with 2-MeV protons. The structure on the high-energy side, shown enlarged in the inset, corresponds to the lines of interest, namely the $K\beta L^1$ satellite and $K\alpha^h$ hypersatellite lines.

state in the K shell, the natural linewidth of the hypersatellite should be much larger than the one of the corresponding diagram line. According to the phenomenological law given by Mossé [10] the natural linewidth of the $K\alpha$ hypersatellite should be equal to $3\Gamma_K + \Gamma_L$. Using tabulated values from Campbell and Papp [11], this simple approximation yields 1.33 eV which is substantially lower than our value.

In further analysis we need to consider that the $1s2p$ state can be produced either by direct ionization or by shake process following the removal of $1s$ electron. For the $1s^2$ state the shake contribution should be approximately an order of magnitude smaller compared to direct ionization [12] so we have neglected it. Therefore direct ionization solely was considered to contribute to the measured $K\alpha$ hypersatellite line intensity, while the $K\beta L^1$ intensity consists from two contributions, direct ionization one and a shake contribution, respectively. The amount of shake contribution in our proton induced $K\beta L^1$ intensity can be estimated by comparing our recently measured $K\alpha L^1$ satellite intensity induced by 1–3-MeV protons [7] with the recent work of Mauron *et al.* [13] where the Si $K\alpha L^1$ shake satellite was found to be $(5.72 \pm 0.03)\%$ of that of the $K\alpha$ diagram line. Using this value and relative intensities of the $K\alpha L^1$ satellite corresponding to direct Coulomb ionization induced in collisions with 1–3-MeV protons (Table 3 in Ref. [7]) we found that 35.9% of the overall $K\alpha L^1$ satellite line intensity measured with 1-MeV, 48.0% with 2-MeV, and 69.6% with 3-MeV protons, respectively, is due to shake processes. Since the $K\beta L^1$ satellite represents a different decay channel of the same initial state these values were adopted also for the $K\beta L^1$ satellite line.

Finally, because of the thick target used in our experiment, we had to account for the proton stopping and x-ray absorption in the target. Since the measured $K\beta L^1$, $K\alpha^h$ lines

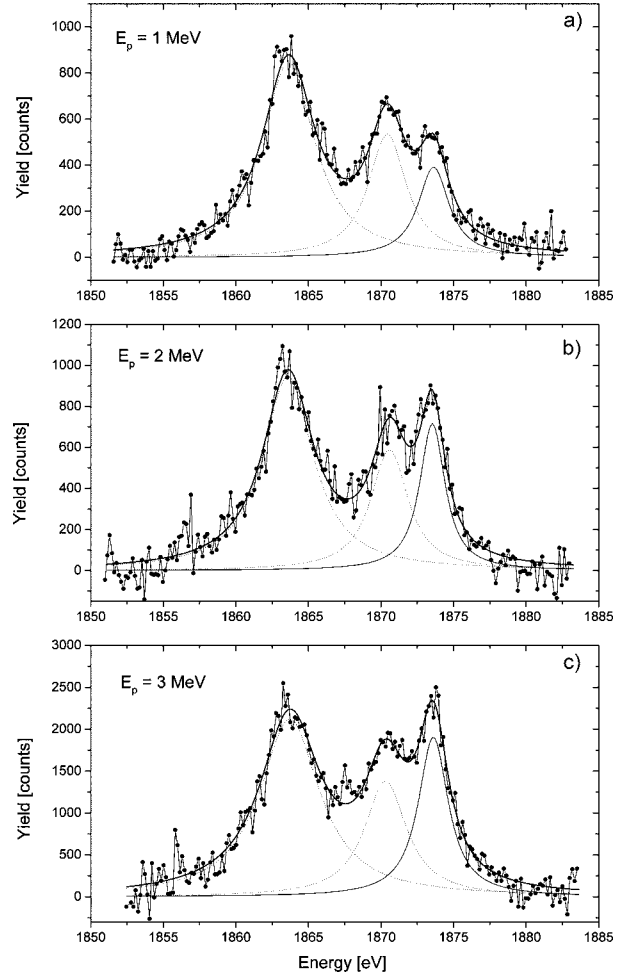


FIG. 2. High-resolution spectra of the $K\beta L^1$ satellite (dotted line) and $K\alpha^h$ hypersatellite lines (solid line) induced in collisions with 1-MeV (a), 2-MeV (b), and 3-MeV (c) protons, respectively. The spectra were decomposed by the fitting model explained in the text. The background described by a second-order polynomial has been subtracted from the spectra before the analysis. As expected the first two lines corresponding to $K\beta L^1$ satellite line show no dependence on the proton energy, while the intensity of the third component corresponding to the hypersatellite line clearly varies with the proton energy.

are situated above the Si K absorption edge (1838.9 eV) only the first few μm below the surface actually contribute to the measured yield due to high self-absorption in the target. Therefore we do not expect this thick target correction to be very significant but we have nevertheless considered it by multiplying the yields by a correction factor defined as follows:

$$F_{corr} = \frac{\sigma_{KK}^{SCA}(E_0)/\sigma_{KL^1}^{SCA}(E_0)}{\int_0^R \sigma_{KK}^{SCA}(E(x)) \exp(-\mu^{KK}x) dx / \int_0^R \sigma_{KL^1}^{SCA}(E(x)) \exp(-\mu^{KL^1}x) dx}, \quad (1)$$

TABLE I. Measured $K\alpha$ hypersatellite to $K\beta L^1$ satellite x-ray yield ratios (second column) and the corresponding yield ratios due to direct ionization solely (fifth column). The relative contributions of the shake process to the measured $K\beta L^1$ x-ray yields and the thick target correction factors are also given.

E_{proton}	$X(K\alpha^h)/X(K\beta L^1)$	$X^{\text{sh}}(K\beta L^1)/X^{\text{total}}(K\beta L^1)$	F_{corr}	$X^{\text{DI}}(K\alpha^h)/X^{\text{DI}}(K\beta L^1)$
1 MeV	(18.6±1.5)%	35.9 %	1.039	(30.1±2.5)%
2 MeV	(25.9±2.0)%	48.0%	1.000	(49.8±4.0)%
3 MeV	(30.6±2.0)%	69.6%	0.986	(99.3±8.8)%

where σ_{KK} and σ_{KL^1} are the ionization cross sections for the K^2 and KL^1 state, respectively, $E(x)$ is the proton energy as a function of the penetration depth x , E_0 is the proton impact energy, R is the range of protons, and μ is the x-ray-absorption coefficient in the Si target. We have used cross sections calculated within the independent electron model incorporating single K and L shell ionization probabilities calculated with the semiclassical approximation (SCA). The $E(x)$ function was calculated using the stopping powers of Ziegler and Manoyan [14] and the x-ray attenuation coefficients for Si were obtained from the tables of Thin and Leroux [15]. As expected, these corrections were very small ranging from <1% for the 2-MeV protons up to 3.9% for the 1-MeV protons.

In Table I we have tabulated the $K\alpha^h/K\beta L^1$ relative x-ray yields extracted from the measured spectra, the estimated ratios of the shake contribution in the $K\beta L^1$ measured yields, the thick target correction factors, and the resulting direct Coulomb ionization $K\alpha^h/K\beta L^1$ relative x-ray yields.

IV. RESULTS AND DISCUSSION

In order to obtain the ratio of the double to single $1s$ ionization cross section for the measured collisions we need to connect our measured relative x-ray yields with the initially populated K^2L^0 , KL^1 vacancy yields. The initial vacancy state production yield ratio $I(K^2L^0)/I(KL^1)$ can be expressed as a function of the corresponding $X(K\alpha^h)$ and $X(K\beta L^1)$ x-ray yields in the following way:

$$\begin{aligned} \frac{X(K\alpha^h)}{X(K\beta L^1)} &= \frac{I(K^2L^0)\omega_{\text{KK}}^\alpha}{I(KL^1)(1-R)\omega_{\text{KL}}^\beta} \Rightarrow \frac{I(K^2L^0)}{I(KL^1)} \\ &= \frac{X(K\alpha^h)}{X(K\beta L^1)}(1-R)\frac{\omega_{\text{KL}}^\beta}{\omega_{\text{KK}}^\alpha}. \end{aligned} \quad (2)$$

The factor R is the rearrangement factor which gives the probability that the L shell vacancy in the atom has been promoted to a higher shell within the lifetime of the KL vacancy state. For Si, $R=0.109\pm 0.033$ [7]. The factors $\omega_{\text{KK}}^\alpha$ and ω_{KL}^β are the $K\alpha$ and $K\beta$ partial fluorescence yields for KK and KL ionized atoms. Since $K\alpha$ transitions represent 98.3% of the total radiative width of the K shell [16] we can approximate $\omega_{\text{KK}}^\alpha=\omega_{\text{KK}}$. The $K\beta$ partial fluorescence yields ω_{KL}^β can be written as

$$\omega_{\text{KL}}^\beta = \omega_{\text{KL}} \frac{\Gamma_{\text{KL}}^\beta}{\Gamma_{\text{KL}}^{\text{rad}}} \approx \omega_{\text{KL}} \frac{\Gamma_{\text{K}\beta}}{(5/6)\Gamma_{\text{K}\alpha}}. \quad (3)$$

Here we have again approximated $\Gamma_{\text{KL}}^{\text{rad}} \approx \Gamma_{\text{KL}}^\alpha$ and in addition we have used the statistical procedure proposed by Larkins [17], in which the additional $2p$ vacancy modifies the $K\alpha$ transition rate by 5/6 due to the reduced number of $2p$ electrons available for the transition, while it does not affect the $K\beta$ transition rate. Equation (2) can now be written as

$$\frac{I(K^2L^0)}{I(KL^1)} = \frac{X(K\alpha^h)}{X(K\beta L^1)}(1-R)\frac{\omega_{\text{KL}}}{\omega_{\text{KK}}}(6/5)\frac{\Gamma_{\text{K}\beta}}{\Gamma_{\text{K}\alpha}}. \quad (4)$$

The total K shell fluorescence yields for multiply ionized Si atom are given by Tunnel and Bhatta [18]. The same value (0.057) for the $1s^2$ and the $1s2p$ ionized Si atom is given. For the ratio of the $K\beta/K\alpha$ transition probabilities Scofield [16] gives a theoretical value of 1.70%. Since the $K\beta$ transitions involve electrons from the valence $3p$ shell significant deviations of the experimental $K\beta/K\alpha$ intensity ratio measured on solid target from the theoretical value can be expected. We have therefore used the experimental value measured with a solid Si target excited with synchrotron radiation with an energy of 1895 eV, which yields a $K\beta/K\alpha$ intensity ratio of $2.10\pm 0.06\%$ [19]. Using this value in Eq. (4) we have determined the $I(K^2L^0)/I(KL^1)$ initial vacancy state production yield ratios and the resulting double to single K shell ionization cross-section ratios, using the following relation:

$$\frac{\sigma_{\text{KK}}}{\sigma_{\text{K}}} = \frac{I(K^2L^0)}{I(KL^0)} = \frac{I(K^2L^0)I(KL^1)}{I(KL^1)I(KL^0)}. \quad (5)$$

The $I(KL^1)/I(KL^0)$ ratios in Eq. (5) were determined from separate $K\alpha$ measurements and are given in Ref. [7]. Finally, the double K shell ionization cross sections were obtained by multiplying the experimental $\sigma_{\text{KK}}/\sigma_{\text{K}}$ ratios with the single K shell ionization cross sections given by Paul and Sacher [20]. The σ_{KK} cross sections together with the initial-state production yield ratios $I(K^2L^0)/I(KL^1)$ obtained in the present work, $I(KL^1)/I(KL^0)$ from Ref. [7], and the σ_{K} cross sections from Ref. [20] are listed in Table II.

We have compared our experimental double $1s$ ionization cross sections with the theoretical predictions calculated within the independent electron approximation. In this approach the double $1s$ shell ionization cross section can be written as

$$\sigma_{\text{KK}} = 2\pi \int_0^\infty p_{\text{K}}^2(b) b db, \quad (6)$$

where $p_{\text{K}}(b)$ is the K shell single electron ionization probability and b is the impact parameter of the projectile. The σ_{KK} cross sections have been obtained within the first-order semiclassical approximation (SCA) employing the SCA calculation of Trautmann and Rösel (IONHYD code) [21] and the SCA calculation of Šmit [22]. They both employ classic hyperbolic trajectories and hydrogenlike Dirac electron wave functions but slightly different approximations are used for the screening of outer atomic electrons. They also differ in the number of multipoles used in the calculation. While

TABLE II. K^2L^0/KL^1 and KL^1/KL^0 vacancy state production yield ratios and resulting double to single $1s$ ionization cross section ratios. Single $1s$ ionization cross sections from Ref. [20] and deduced double $1s$ shell ionization cross sections are also given.

E_{proton}	$I(K^2L^0)/I(KL^1)$	$I(KL^1)/I(KL^0)$ [7]	σ_{KK}/σ_K	σ_K [kbarn] [20]	σ_{KK} [barn]
1 MeV	$(68 \pm 7) \times 10^{-4}$	$(10.6 \pm 1.7)\%$	$(7.2 \pm 1.3) \times 10^{-4}$	10.27	7.4 ± 1.4
2 MeV	$(112 \pm 11) \times 10^{-4}$	$(6.4 \pm 1.0)\%$	$(7.2 \pm 1.3) \times 10^{-4}$	19.48	14.0 ± 2.6
3 MeV	$(223 \pm 23) \times 10^{-4}$	$(2.6 \pm 0.5)\%$	$(5.8 \pm 1.3) \times 10^{-4}$	22.74	13.2 ± 2.9

IONHYD code calculates multipoles up to the order $l=5$, in the calculation of \check{S} mit only multipoles up to $l=2$ were considered.

In order to evaluate both models we have first calculated the single $1s$ ionization cross sections of Si induced in collisions with protons and compare the calculated curves with the cross sections of Paul and Sacher [20]. This comparison is presented in Fig. 3. Both calculations generally reproduce rather well the energy dependence but the calculation of \check{S} mit matches better the reference cross sections. The underestimation of the cross sections by \check{S} mit's calculation at higher energies could be at least partially explained by the nonconsideration of the higher multipoles which should increase the calculated values by approximately 6–7 %.

The same two calculations were then used to determine the double $1s$ ionization cross sections. Also in this case the energy dependence is reproduced quite well but the absolute values are overestimated significantly. This kind of discrepancies were already observed for some other low-Z (Ca-Cr) [4] and also some mid-Z elements [5]. To reduce these discrepancies a two step model for the double $1s$ ionization was suggested. In this model the screening and the binding energy of the second electron are changed after the ejection of the first $1s$ shell electron. The double $1s$ ionization cross section can be therefore written as

$$\sigma_{KK}^* = 2\pi \int_0^\infty p_K(b) p_K^*(b) b db, \quad (7)$$

where $p_K^* < p_K$ due to the ejection of the first electron. We have calculated also the two-step cross sections for both

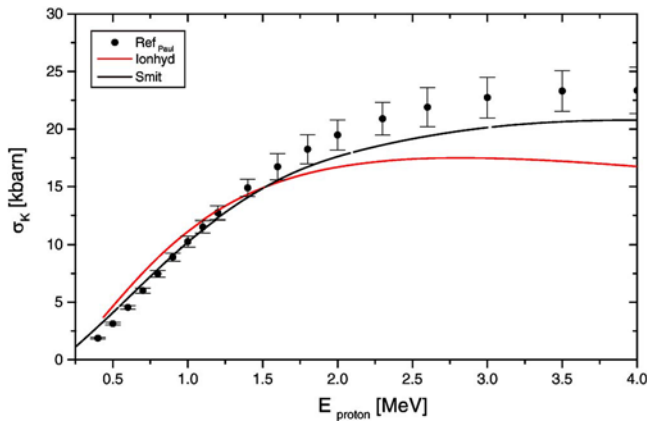


FIG. 3. (Color online) The single $1s$ ionization cross sections of Si bombarded with protons from Ref. [20] compared with the first-order SCA calculation of Trautmann and Rösél [21] (red line) and the SCA calculation of \check{S} mit [22] (black line).

SCA calculations. The increase of the binding energy for the second $1s$ electron was set to 183 eV calculated with the Hartree-Fock model and the charge of the bare nucleus was considered to calculate p_K^* . The calculated σ_{KK}^* was found to be 10–20 % smaller than the σ_{KK} therefore reducing the discrepancies with our experimental values, but still the calculations overestimate our experimental cross sections. The comparison of our experimental double $1s$ ionization cross sections with the SCA calculated σ_{KK} and σ_{KK}^* values is presented in Fig. 4.

Finally the assumption of the sequential two step model for the double $1s$ ionization suggested also by the comparison of our data with the SCA calculations have been further tested using a four-body classical trajectory Monte Carlo (CTMC) calculations. In this CTMC approach, classical non-relativistic equations of motion for a four body system are solved numerically for a statistically large number of trajectories. The four particles of given masses and charges interact with each other via the Coulomb interaction except for the two electrons, following from the concept of independent electrons. The impact parameter of the projectile and the orientation and velocity of the electrons moving around the target nucleus are randomly selected according to the Monte Carlo method. More details about the used method can be found in Ref. [23]. At low energies below 1 MeV the CTMC

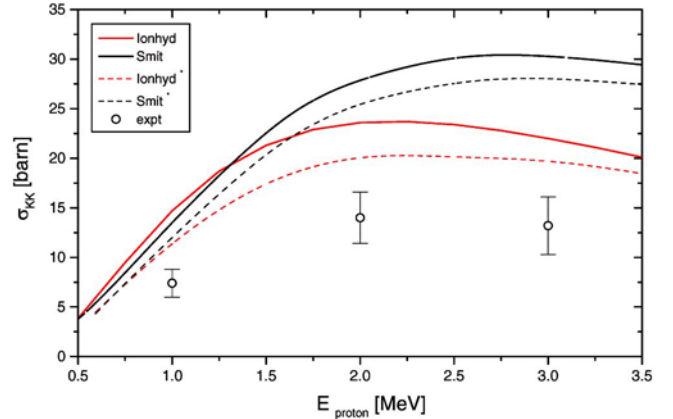


FIG. 4. (Color online) Double $1s$ direct ionization cross sections σ_{KK} as a function of the proton energy. Our experimental results are compared with the theoretical calculation within the independent electron framework using single electron ionization probabilities calculated by the first-order SCA calculation of Trautmann and Rösél [21] (red line) and the SCA calculation of \check{S} mit [22] (black line). The dashed curves represent the double ionization cross sections σ_{KK}^* calculated with the two step model where the binding energy of the second $1s$ electron is increased.

3 MeV H^+ + Si($1s^2$), $b=0.05$ a.u.

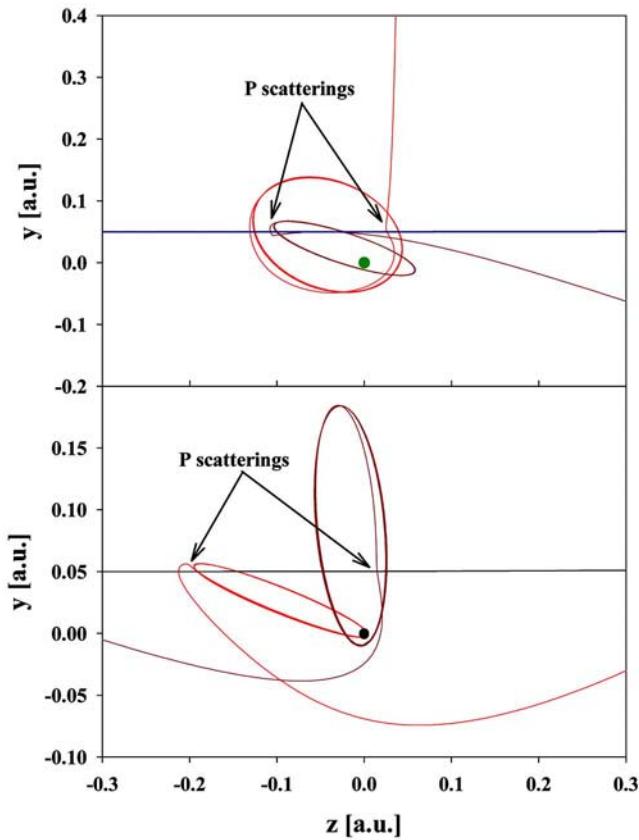


FIG. 5. (Color online) Two typical trajectories for the double $1s$ ionization of Si calculated for the 3-MeV proton at an impact parameter of 0.05 atomic unit. The trajectories of projectile (straight solid line) and both $1s$ electrons together with the position of the target nucleus (solid dot) are presented in the laboratory frame and in an arbitrary plane (y - z) projection. The positions of the ejection of first and second $1s$ electron along the projectile's trajectory are indicated with arrows. Calculated trajectories demonstrate the sequential two step process leading to the ejection of both $1s$ electrons.

absolute double $1s$ ionization cross sections are slightly lower than the SCA ones but at higher energies they are much larger than the SCA values. The difference increases with the increasing proton energy and start to level out around 4 MeV where it reaches three to four times larger σ_{KK} values than the SCA ones. A more detailed comparison of the different models used in these calculations will be

presented elsewhere [24]. Here the primary aim of the CTMC calculation was to probe the validity of the two step model for the description of double $1s$ ionization. For this purpose two typical trajectories for the double $1s$ ionization of a Si atom colliding with a 3-MeV proton are presented in Fig. 5. Calculated trajectories clearly exhibit a two step ionization process proving therefore the validity of the sequential two step model for the description of the double $1s$ ionization in such ion atom collisions.

V. SUMMARY AND CONCLUSION

In this work the double $1s$ ionization of Si induced in collisions with 1–3-MeV protons has been studied experimentally and theoretically. Using a high-resolution crystal spectrometer in Johannsson geometry the $K\alpha^h$ hypersatellite lines corresponding to the $1s^2 \rightarrow 1s2p$ transitions were measured and their intensities relative to the $K\beta L^1$ satellite determined. From these relative intensities the ratios of the double to single $1s$ ionization cross sections due to direct Coulomb ionization were determined for the three studied collisions. Multiplying the cross-section ratios with the experimental single $1s$ ionization cross sections, absolute values for the double $1s$ ionization cross sections could be obtained. The experimental values were compared with results of theoretical calculations based on the independent electron model, using single $1s$ electron ionization probabilities calculated within the semiclassical approximation. This theory was found to reproduce well the experimental single $1s$ ionization cross sections, while overestimating significantly the measured double $1s$ cross section. A part of these discrepancies could be removed by employing a two step sequential model for the calculation of the double ionization. The validity of the two step process has been finally confirmed by four body classical trajectory Monte Carlo calculations, the latter exhibiting clearly the sequential two step double $1s$ ionization events.

ACKNOWLEDGMENTS

M.K. would like to thank P. Pelicon and Z. Grabnar for providing good beam conditions, Ž. Šmit for useful discussions about the SCA calculations, and J.-Cl. Dousse for his help in preparation of the manuscript. This work was supported by the Slovenian Ministry of Education, Science and Sport through the research program “Low Energy Physics” (PO-0521-0106-02), by the Swiss National Science Foundation, and through a bilateral Scientific and Technological Cooperation between Slovenia and Hungary (Project No. BI-HU/04-05-013).

- [1] P. Richard, W. Hodge, and C. F. Moore, Phys. Rev. Lett. **29**, 393 (1972).
- [2] J. Hall, P. Richard, T. J. Gray, C. D. Lin, K. Jones, B. Johnson, and D. Gregory, Phys. Rev. A **24**, 2416 (1981).
- [3] J. Hall, P. Richard, P. L. Pepmiller, D. C. Gregory, P. D. Miller, C. D. Moak, C. M. Jones, G. D. Alton, L. B. Bridwell, and C.

J. Scofield, Phys. Rev. A **33**, 914 (1986).

- [4] V. Cindro, M. Budnar, M. Kregar, V. Ramšak, and Ž. Šmit, J. Phys. B **22**, 2161 (1989).
- [5] B. Boschung, J.-Cl. Dousse, B. Galley, Ch. Herren, J. Hoszowska, J. Kern, Ch. Rhême, Z. Halabuka, T. Ludziejewski, P. Rymuza, Z. Sujkowski, and M. Polasik, Phys. Rev. A **51**, 3650

(1995).

- [6] M. Kopal, M. Kavčič, M. Budnar, J.-Cl. Dousse, Y.-P. Mailard, O. Mauron, P.-A. Raboud, and K. Tökési, *Phys. Rev. A* **70**, 062720 (2004).
- [7] M. Kavčič, *Phys. Rev. A* **68**, 022713 (2003).
- [8] R. D. Deslattes, E. G. Kessler, Jr., P. Indelicato, L. de Billy, E. Lidroth, and J. Anton, *Rev. Mod. Phys.* **75**, 35 (2003).
- [9] M. C. Martins, A. M. Costa, J. P. Santos, F. Parente, and P. Indelicato, *J. Phys. B* **37**, 3785 (2004).
- [10] J. P. Mossé, P. Chevallier, and J. P. Briand, *Z. Phys. A* **322**, 207 (1979).
- [11] J. L. Campbell, and T. Papp, *At. Data Nucl. Data Tables* **77**, 1 (2001).
- [12] T. Mukoyama, and K. Taniguchi, *Phys. Rev. A* **36**, 693 (1987).
- [13] O. Mauron, J.-Cl. Dousse, J. Hozzowska, J. P. Marques, F. Parente, and M. Polasik, *Phys. Rev. A* **62**, 062508 (1998).
- [14] J. F. Ziegler and J. Manoyan, *Nucl. Instrum. Methods Phys. Res. B* **35**, 215 (1988).
- [15] T. P. Thinh and J. Leroux, *X-Ray Spectrom.* **8**, 85 (1979).
- [16] J. H. Scofield, *At. Data Nucl. Data Tables* **14**, 121 (1974).
- [17] F. P. Larkins, *J. Phys. B* **4**, L29 (1971).
- [18] T. W. Tunnel and C. P. Bhalla, *Phys. Lett.* **86A**, 13 (1981).
- [19] J. Szlachetko (private communication).
- [20] H. Paul, and J. Sacher, *At. Data Nucl. Data Tables* **42**, 105 (1989).
- [21] D. Trautmann and F. Rösel, *Nucl. Instrum. Methods* **169**, 259 (1980).
- [22] Ž. Šmit, *Phys. Rev. A* **53**, 4145 (1996).
- [23] K. Tökési, and G. Hock, *J. Phys. B* **29**, L119 (1996).
- [24] K. Tökési, and M. Kavčič (unpublished).